Molecular Crystals and Liquid Crystals Science and Technology. Section A. Molecular Crystals and Liquid Crystals
Publication details, including instructions for authors and subscription information:
http://www.tandfonline.com/loi/gmcl19

Experimental Data and Modelling of the Interactions in Solid State and in Solution between (R) and (S) N-Acetyl-α-Methylbenzylamine. Influence on Resolution by Preferential Crystallization

S. Druot [a] , M. N. Petit [a] , S. Petit [b] , G. Coquerel [b] & N. B. Chanh [c]
[a] Laboratoire de Chimie Minérale et Structurale, 76821, Mont Saint Aignan Cedex, France
[b] Laboratoire de Modélisation Moléculaire, Centre de Spectroscopic, I. F. R.M.P., 76821, Mont Saint Aignan Cedex, France
[c] Laboratoire de Cristallographie et de Physique Cistalline, ERS133, 351, Cours de la Libération, 33405, Talence Cedex, France
Version of record first published: 24 Sep 2006.

To cite this article: S. Druot , M. N. Petit , S. Petit , G. Coquerel & N. B. Chanh (1996): Experimental Data and Modelling of the Interactions in Solid State and in Solution between (R) and (S) N-Acetyl-α-Methylbenzylamine. Influence on Resolution by Preferential Crystallization, Molecular Crystals and Liquid Crystals Science and Technology. Section A. Molecular Crystals and Liquid Crystals, 275:1, 271-291

To link to this article: http://dx.doi.org/10.1080/10587259608034081

Mol. Cryst. Liq. Cryst., 1996, Vol. 275, pp. 271–291
Reprints available directly from the publisher
Photocopying permitted by license only

Experimental Data and Modelling of the Interactions in Solid State and in Solution between (R) and (S) *N*-Acetyl-α-Methylbenzylamine. Influence on Resolution by Preferential Crystallization

S. DRUOT and M. N. PETIT

Laboratoire de Chimie Minérale et Structurale, 76821 Mont Saint Aignan Cedex, France

and

S. PETIT and G. COQUEREL

Laboratoire de Modélisation Moléculaire, Centre de Spectroscopie, I.F.R.M.P., 76821 Mont Saint Aignan Cedex, France

and

N. B. CHANH

Laboratoire de Cristallographie et de Physique Cistalline, ERS133, 351, Cours de la Libération, 33405 Talence Cedex, France

(Received January 18, 1995)

The binary phase diagram between (R) and (S) *N*-acetyl-α-methylbenzylamine has been established by using differential scanning calorimetry and X-ray diffraction. Up to 337 K, the two enantiomers form an eutectic mixture without partial solid solution (i.e. conglomerate). At 337 K, the eutectoid equilibrium: conglomerate⇔racemate ($\Delta H \geq 1.25\,kJ\cdot mol^{-1}$) is observed. Several hypotheses are made about the upper part ($T > 340\,K$) of the binary diagram to explain the complex succession of stable and metastable thermal phenomena.

The structures of enantiomer and metastable racemate have been solved by X-ray diffraction on single crystals at 293 K. Infinite Chains of H-bonded Molecules (CHBMs) exist in the two structures: isotactic in enantiomer and syndiotactic in racemate. M.O. calculations (PM3) show that conformation of the molecule in enantiomer structure is more stable by $9.4\,kJ\cdot mol^{-1}$ than the conformation of the molecule in racemate. The other energy differences (H-bonds and van der Waals contacts) between the two structures do not reverse the order of relative stabilities.

Two isothermal solubility studies at 273 K and 287 K have been carried out in the system: (R)-(S)-toluene and in the system: (R)-(S)-acetonitrile. In toluene, a significant departure from the ideal behaviour appears when temperature increases from 273 K upwards. A hypothesis involving a dynamic equilibrium between solvated CHBMs containing *n* monomers is postulated, the *n* value being dependent on the temperature and nature of the solvent. The more the optical purity departs from 100%, the more atactic the CHBMs and the weaker the interactions between these chains. The strength of the interactions between CHBMs versus the optical purity and the temperature seems to be responsible for the departure from the ideal behaviour.

The homogeneous nucleation of the metastable racemate at 293 K, in highly supersaturated racemic solution, is discussed in terms of diffusion of molecules in solution.

Preferential crystallization has been achieved in toluene and acetonitrile, but the difficulties which arose in its implementation appear to be roughly independent of the solvent and are connected to R⇔S interactions at the crystal-solution interface as soon as the composition of the solution departs from racemic.

Keywords: Enantiomers and racemates, binary and ternary phase diagrams, crystal structures, preferential crystallization, MO calculations, interactions in solid state and in solutions

1. INTRODUCTION

Besides the asymmetric synthesis of optically pure substances, the resolution of racemic mixtures is still widely used, mainly because of its economic interest. Among the processes of resolution currently used, preferential crystallization is attractive because of the following advantages:

- The theoretical yield is 100% by means of successive recycling of the mother liquors,
- No chiral resolving agent is needed,
- The purification of the crude enantiomers obtained at each run is easy to perform.

However, its applicability requires the stability of the conglomerate versus the racemate in the used solvent, and usually only 5 to 10% of the racemic mixtures crystallize as a conglomerate. In addition to this essential condition, some problems during the entrainment itself have also been reported. They result from R-S interactions because of the incorporation of the counter enantiomer as a crystal defect in the lattice[1,2] or the irreversible inhibition of crystal growth within the limits of acceptable supersaturation.[3]

Despite α-methylbenzylamine being the most widely used as resolving agent,[4] the resolution of its derivatives by preferential crystallization has not yet attracted a lot of attention, and only a few studies report the application of the method.[5,6] The mitigated results obtained in these previous studies led us to reconsider the resolution of the (±) *N*-acetyl-α-methylbenzylamine (NACMBA hereafter, Figure 1) described in the literature as crystallizing as a conglomerate.[7] Before any study of the kinetic conditions of crystallization, knowledge of the heterogeneous equilibria between the two enantiomers in the binary system and in the ternary system (i.e. with a solvent) is necessary. The aim of this study is also to investigate the interactions between opposite enantiomers and their consequences on preferential crystallization.

2. EXPERIMENTALS AND RESULTS

2.1 Synthesis of (±) and (R) NACMBA

Racemic or optically pure amine base (Aldrich 99%) dissolved in dichloromethane is slowly supplemented with acetylchloride in small excess (3%). In order to remove the unreacted components, the solution is successively washed with acidic and basic aqueous solutions. The resulting liquor is dried with magnesium sulfate and evaporated (yield > 90%); (±)-NACMBA (or (R)-NACMBA) is then recrystallized twice from toluene.

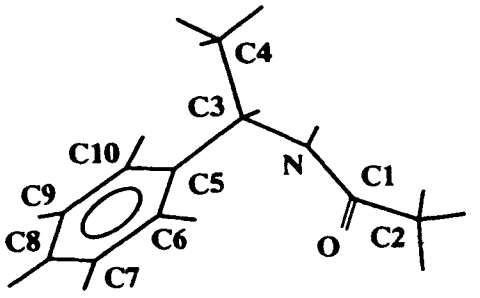

FIGURE 1 Structural formula of *N*-acetyl-α-methyl-benzylamine (NACMBA).

Specific optical values of (R) pure enantiomer are determined in ethanol (c = 1 g/100 ml, 293 K) for various wavelengths:

λ(nm)	589	578	546	436	365
[α](°)	+151	+158	+182	+339	+599

2.2 Binary System (R)-NACMBA-(S)-NACMBA and Identification of Phases

The heterogeneous equilibria have been investigated by means of DSC (differential scanning calorimetry, Setaram 101) with the following procedure. Each mixture of known composition between (±) and (R) was finely ground in a mortar. Between 20 to 24 mg of this mixture was introduced in an aluminium crucible and heated at the 2 K·min^{-1} constant rate from room temperature to complete fusion under a constant flow of nitrogen. All temperatures and enthalpies were corrected according to values obtained from known pure standards.

2.2.1 Phase Identification in Binary System

Figure 2 depicts the DSC curve of the racemic mixture on heating: the first endothermic peak at 337 K does not appear on the DSC curve of the enantiomer, showing that this phenomenon is different from the polymorphism of the enantiomers (this peak would have revealed the four-phase invariant predicted by Scott[8] but not yet experimentally detected); it corresponds to the reversible and stable three-phase equilibrium (eutectoid type) conglomerate–racemate: $\langle R\rangle + \langle S\rangle \Leftrightarrow \langle RS\rangle$ (ΔH = 1.25 kJ·mol^{-1}).

The second peak can be divided into two poorly separated signals. Several experiments carried out with different heating rates, with or without annealing at 344 K, did not result in a better resolution. This kind of melting peak is quite common among the organic compounds and sometimes it may be attributed to polymorphism. Thus, from the DSC study, the racemate might exist in two forms (I and II) with close melting points, but no transition temperature is detected.

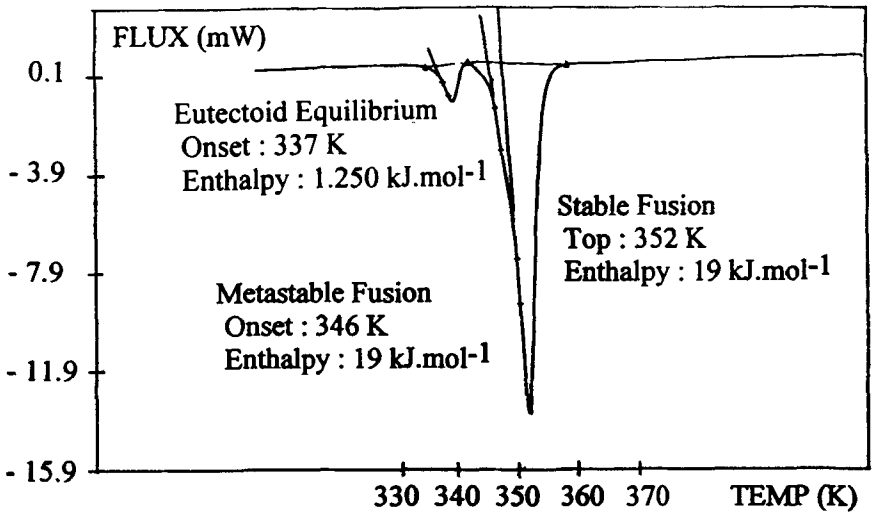

FIGURE 2 DSC curve for (±) NACMBA (heating rate: 2 K·min^{-1}).

Figure 3 shows the powder X-ray diffraction pattern, obtained with a Guinier-Simon camera, of the racemic mixture on being heated from 293 K to 393 K. The sample, put in a sealed Lindemann capillary ($\varnothing = 0.5$ mm), was heated at the rate of 0.07 K·min^{-1}. From this experiment, we confirm the existence of the conglomerate below 337(± 3) K and the stability of the racemate above this temperature. Nevertheless, we cannot confirm the polymorphism of the racemate at higher temperature.

The two isolated solids are identified by their powder X-ray diffraction patterns, collected on a D500 Siemens diffractometer (Table I), at the following temperatures: $T = 293$ K for the enantiomer and $T = 346$ K for the racemate. From these data, the indexings and refinements were achieved using the programs DICVOL91[9] and AF-MAIL. The final unit cell parameters are:

- Enantiomer at 293 K: tetragonal, $a = b = 6.7533(3)$ Å, $c = 41.883(13)$ Å, $V = 1910(3)$ Å^3, $Z = 8$, $F_{20} = 19$, $M_{20} = 12$.
- Racemate at 346 K: monoclinic, $a = 11.311(4)$ Å, $b = 9.654(4)$ Å, $c = 9.578(4)$ Å, $\beta = 108.55(3)°$, $V = 992(3)$ Å^3, $Z = 4$, $F_{22} = 25$, $M_{22} = 13$.

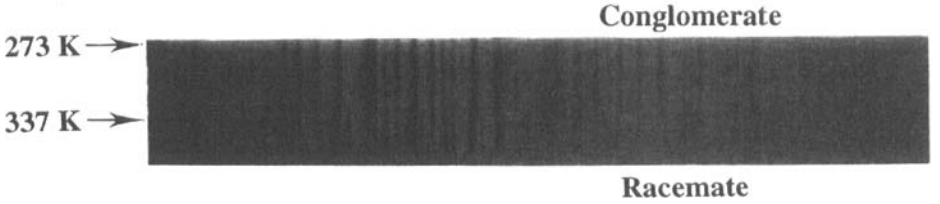

FIGURE 3 X-Ray diffraction pattern of NACMBA conglomerate undergoing a heating process.

TABLE I

Power X-ray diffraction data for conglomerate and racemate of NACMBA

Conglomerate ($T = 293$ K)				Racemate ($T = 346$ K)			
h k l	d_{calc}(Å)	d_{obs}(Å)	I/I_0	h k l	d_{calc}(Å)	d_{obs}(Å)	I/I_0
0 0 4	10.47	10.35	100	1 0 0	10.72	10.69	2
1 0 2	6.43	6.42	4	1 1 0	7.17	7.18	16
1 0 3	6.08	6.08	5	1 1 −1	6.32	6.34	10
1 0 4	5.675	5.680	8	2 0 0	5.361	5.363	100
0 0 8	5.235	5.212	56	1 1 1	5.124	5.121	19
1 1 1	4.744	4.743	12	2 1 0	4.687	4.687	14
1 1 2	4.656	4.656	20	0 0 2	4.540	4.535	20
1 1 3	4.518	4.514	2	1 2 0	4.402	4.401	6
1 1 4	4.345	4.342	6	0 2 1	4.262	4.261	12
1 1 5	4.148	4.143	42	2 0 −2	4.183	4.185	19
1 1 6	3.941	3.943	12	0 1 2	4.109	4.104	9
1 0 9	3.832	3.834	13	2 1 −2	3.838	3.838	17
1 1 7	3.732	3.735	7	2 1 1	3.761	3.757	14
1 0 10	3.559	3.556	23	2 2 −1	3.609	3.604	25
1 1 8	3.528	3.530	28	3 0 0	3.574	3.577	20
2 0 2	3.333	3.337	9	3 1 −1	3.502	3.505	8
1 1 9	3.332			3 0 −2	3.379	3.382	13
1 1 11	2.977	2.977	6	3 1 0	3.352	3.346	18
1 0 13	2.908	2.910	5	1 0 −3	3.190		
1 1 12	2.818	2.819	6	3 1 −2	3.189	3.189	5
1 0 14	2.735	2.737	6	2 2 −2	3.161	3.159	4
1 1 13	2.671	2.674	5	0 0 3	3.027		
0 0 16	2.617	2.617	9	2 0 2	3.023	3.022	3
1 0 15	2.580	2.585	2	3 2 −1	2.966	2.963	6
1 1 14	2.535	2.538	6				
1 2 9	2.533						
1 0 16	2.441	2.442	11				

2.2.2 *Binary Diagram and Interpretation*

Figure 4a shows the experimental binary phase diagram between the two enantiomers. In addition to the eutectoid invariant at 337 K, a metastable eutectic at 346 K and a stable eutectic at 350 K appear. The calculated eutectic temperatures and compositions using Prigogine-Defay-Mauser expression[10] for the racemate and Schröeder-Van Laar[11,12] for the enantiomers lead to:

- A stable eutectic between enantiomer and racemate at $T = 348$ K, $C_R = 44$ and 56%, these values are in good agreement with the experimental data (350 K, $C_R = 45$ and 55%).
- A metastable eutectic between the enantiomers (i.e. conglomerate) at 344 K.

Because of the proximity of several heterogeneous phenomena, these experimental and calculated data led us to formulate three hypotheses concerning the metastable eutectic although we were unable to choose between them.

1. Due to the poor diffusion rate is solids, the eutectoid transition is not complete and the remaining parts of R and S enantiomers melt as soon as the temperature of fusion of the conglomerate is reached (Figure 4b). In this case, the enthalpy of

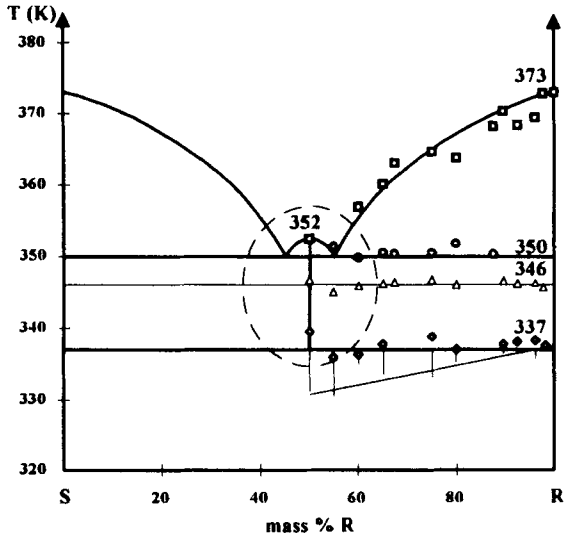

Caption :
- O Stable melting eutectic
- Δ Metastable melting eutectic
- ◊ R + S ⇔ RS eutectoid
- □ End of melting
- —— Stable equilibria
- —— Metastable equilibria

FIGURE 4a Experimental binary phase diagrams between (R) and (S) *N*-acetyl-α-methylbenzylamine.

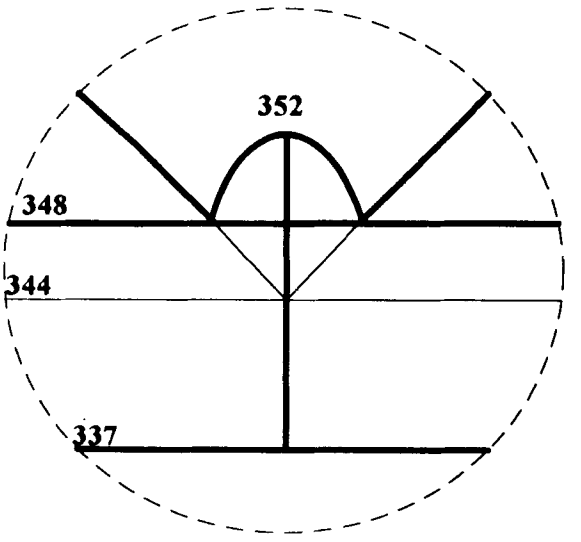

FIGURE 4b Possible identification of the metastable eutectic at 346 K as the metastable conglomerate.

the eutectoid invariant has been underestimated and thus $\Delta H > 1.25\,kJ \cdot mol^{-1}$.

2. The racemate has two polymorphic forms, the metastable equilibrium is the eutectic between the monotropic variety (form I) of the racemate and the enantiomer R or S (Figure 4c). Neither the exothermic peak associated with the transition: Racemate (form I) → Racemate (form II), nor the X-ray pattern of racemate (form II) have been observed. The activation energy of this transition could also be too high, so that form I transforms into form II via the liquid phase just before the stable eutectic.
3. The racemate also has two polymorphic forms, the metastable equilibrium is the eutectic between the enantiotropic modification (form I) of the racemate and the enantiomer R or S (Figure 4d). In that case, the polymorphic transition: Racemate (form I) ⇔ Racemate (form II) has not been detected but should exist. It would have been detected through an endothermic peak if the transition rate had been high enough and not too close to the temperature of the stable eutectic.

2.3 Crystal Structures

2.3.1 Preparation of single crystals, data collections and resolutions of the structures

Single crystals of sufficient size were obtained by slow (enantiomer) or fast (racemate) evaporation at 293 K, of a solution of (R) NACMBA (enantiomer) of (±) NACMBA (racemate) in toluene. Diffracted intensities were measured with automatic diffractometers Enraf-Nonius, CAD3 (enantiomer) or CAD4 (racemate), at room tempera-

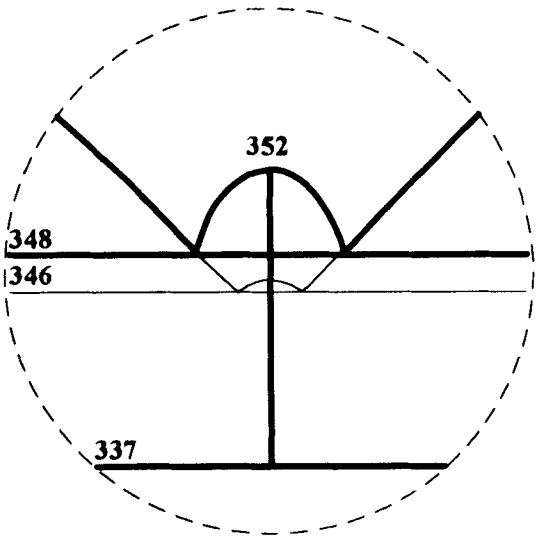

FIGURE 4c Possible identification of the metastable eutectic at 346 K involving a monotropic form of the racemate.

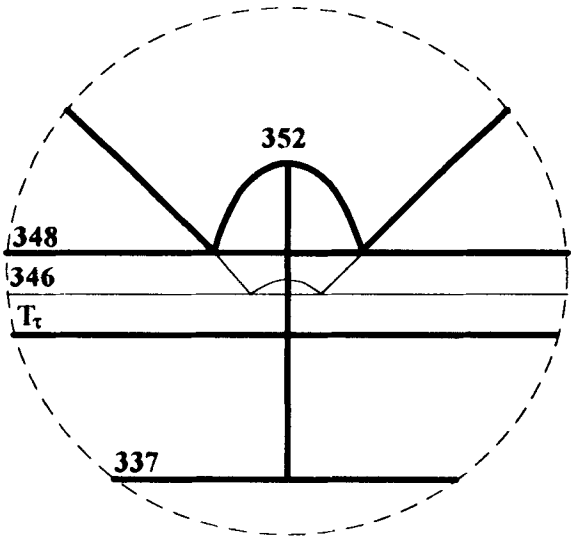

FIGURE 4d Possible identification of the metastable eutectic at 346 K involving an enantiotropic form of the racemate.

ture. The unit-cells found are consistent with the indexings of the powder X-ray diffraction patterns. The crystallographic parameters, as well as the conditions of data collections and refinements of the structures, are detailed in Table II.

The structures were solved using direct methods (SHELXS[13]). The best solutions allowed the 12 non-hydrogen atoms to be located approximately. During the least-squares refinements, the coordinates of all hydrogen atoms were successively obtained from difference-Fourier syntheses. The last refinements were realized with anisotropic thermal parameters assigned to all non-hydrogen atoms. Table III contains final atomic coordinates. Pertinent distances, angles and torsion angles are summarized in Table IV.

2.3.2 *Description of the (R) enantiomer structure*

The side chain plane (Figure 1) defined by C2, C1, O, N and C3 atoms (rms = 2.0 E^{-2}) is 86.2° from the phenyl ring plane (rms = 1.6 E^{-3}); C4 atom is 0.54 Å from the side chain plane. The strongest intermolecular link is a hydrogen bond between N—H···O atoms: d(N—O) = 2.86 Å; d(H···O) = 2.03 Å; (N—H···O) = 175.0°. As a consequence, the main feature of the structure (Figure 5) is infinite and isotactic Chains of H-Bonded Molecules (CHBMs) alternately parallel to ⟨110⟩ and ⟨1–10⟩ in successive (004) slices. The side chains involved in CHBMs form a corrugated series of planes which are 25.7° apart, with the row ⟨441⟩ as a common edge.

Successive (004) slices are held together mainly by φ-φ interactions (Figure 6), and some van der Waals contacts ensure the cohesion between the parallel CHBMs inside the (004) slices.

TABLE II

Crystallographic characteristics, conditions of measurement, structure solutions and refinement parameters for (R) NACMBA and (rac) NACMBA

	(R) NACMBA	(rac) NACMBA
Formula	$C_{10}H_{13}NO$	$C_{10}H_{13}NO$
Fw(g)	163.22	163.22
a(Å)	6.748(2)	11.209(4)
b(Å)	6.748(2)	9.519(3)
c(Å)	41.815(12)	9.569(3)
α(°)	90	90
β(°)	90	108.53(2)
γ(°)	90	90
V(Å^3)	1904(2)	968(2)
Space group	$P4_12_12$	$P2_1/c$
Z	8	4
Crystal shape	Truncated pyramid	Elongated needle along $\vec{c}$
Crystal colour	Colourless	Colourless
μ(cm^{-1})	5.10	0.69
Density ρ_{calc}(g·cm^{-3})	1.14	1.13
Diffractometer	CAD3 Enraf-Nonius	CAD4 Enraf-Nonius
Radiation	Cu Kα(λ = 1.5418 Å)	Mo Kα(λ = 0.7107 Å)
Scan type	$\theta/2\theta$	$\omega/2\theta$
Scan range (°)	$0.9 + 0.3\,\mathrm{tg}\theta$	$0.8 + 0.345\,\mathrm{tg}\theta$
θ limits (°)	0–35	1–25
T(K)	293(1)	293(1)
h, k, l range	(−8, +8)(−8, +1)(−49, +42)	(−11, +11)(0, +9)(0, +9)
Measured reflexions	6210	1890
Unique reflexions	4810	1674
Data used for refinement	2284[$F_0^2 > 4\sigma(F_0)^2$]	712[$(F_0)^2 > 3\sigma(F_0)^2$]
R(int)	0.051	0.024
$R = \Sigma[F_0) - (F_c)]/\Sigma(F_0)$	0.037	0.048
$Rw = \Sigma w[(F_0) - (F_c)]^2/\Sigma w F_0^2$	0.037(w = 1)	0.042(w = 1.0)
Absorption correction	no	DIFABS (min = 0.91, max = 1.09)
Nb of variables	149	149
$\Delta\rho_{min}$(e/Å^3)	−0.30	−0.15
$\Delta\rho_{max}$(e/Å^3)	0.21	0.13

2.3.3 *Description of the racemate structure*

The side chain plane (rms = 1.4 E^{-2}) is 88.80° from the phenyl ring plane (rms = 5.3 E^{-3}); C4 atom is 0.62 Å from the side chain plane (Figure 7). The hydrogen bond has almost the same characteristics as in the structure of the enantiomer: d(N—O) = 2.87 Å, d(H···O) = 2.10 Å; (N—H···O) = 171.8°; nevertheless, the resulting CHBMs are syndiotactic. They have the same periodicity (c = 9.471 Å at 293 K) as in the enantiomer structure ($2d_{110}$ = 9.543 Å at 293 K). The side chain planes of successive molecules are rotated around c axis by alternately + 34° or − 34° from the (100) plane. The CHBMs are held together by van der Waals contacts; in the slice (002) of F type,[14] these contacts are between homochiral molecules exclusively. At 293 K, the two packings have almost the same compacity as it could be seen through the values of density ρ: ρ(rac) = 1.13, ρ(enant) = 1.14; nevertheless, there is a slight advantage for the enantiomer, in opposition to Wallach's rule.[15]

TABLE III

Fractional atomic coordinates and equivalent isotropic thermal parameters (Å^2) for (R) NACMBA and (rac) NACMBA

	(*R*) NACMBA				(rac) NACMBA			
Atom	*x/a*	*y/b*	*z/c*	U_{eq}(Å^2)	*x/a*	*y/b*	*z/c*	U_{eq}(Å^2)
C(1)	0.6832(4)	0.1794(4)	−0.0065(1)	0.0471	0.2369(4)	−0.3132(5)	0.7083(5)	0.0599
C(2)	0.8442(4)	0.1439(4)	−0.0306(1)	0.0740	0.1625(6)	−0.4204(6)	0.6010(6)	0.0841
C(3)	0.5793(3)	0.3764(3)	0.0391(1)	0.0407	0.3634(4)	−0.1010(5)	0.7459(5)	0.0675
C(4)	0.6335(4)	0.5824(3)	0.0515(1)	0.0530	0.4601(6)	−0.0483(7)	0.6768(8)	0.0971
C(5)	0.5639(4)	0.2335(3)	0.0668(1)	0.0345	0.2808(4)	0.0182(5)	0.7648(5)	0.0579
C(6)	0.7222(4)	0.1252(4)	0.0778(1)	0.0439	0.1576(5)	0.0321(6)	0.6803(6)	0.0805
C(7)	0.7041(4)	0.0033(4)	0.1042(1)	0.0542	0.0843(6)	0.1424(8)	0.7013(8)	0.1054
C(8)	0.5286(5)	−0.0101(3)	0.1194(1)	0.0595	0.1337(9)	0.2374(7)	0.8080(1)	0.1073
C(9)	0.3693(4)	0.0972(4)	0.1089(1)	0.0660	0.2544(9)	0.2255(8)	0.8947(9)	0.1073
C(10)	0.3862(4)	0.2178(3)	0.0827(1)	0.0498	0.3286(6)	0.1163(7)	0.8749(7)	0.0951
O	0.5262(3)	0.0906(2)	−0.0073(1)	0.0694	0.2442(3)	−0.3183(4)	0.8406(3)	0.0819
N	0.7256(3)	0.3167(3)	0.0153(1)	0.0445	0.2929(3)	−0.2149(4)	0.6553(4)	0.0617
H(21)	0.797	0.160	−0.052	0.050	0.162	−0.404	0.508	0.120
H(22)	0.882	0.015	−0.032	0.050	0.194	−0.504	0.648	0.120
H(23)	0.953	0.228	−0.029	0.050	0.071	−0.402	0.587	0.120
H(3)	0.445	0.385	0.028	0.050	0.411	−0.147	0.856	0.120
H(41)	0.526	0.626	0.067	0.050	0.425	−0.014	0.570	0.120
H(42)	0.754	0.578	0.063	0.050	0.519	−0.125	0.679	0.120
H(43)	0.637	0.675	0.034	0.050	0.503	0.039	0.720	0.120
H(6)	0.849	0.127	0.065	0.050	0.123	−0.034	0.601	0.120
H(7)	0.812	−0.066	0.112	0.050	−0.004	0.150	0.638	0.120
H(8)	0.521	−0.085	0.136	0.050	0.092	0.310	0.818	0.120
H(9)	0.266	0.077	0.117	0.050	0.300	0.281	0.961	0.120
H(10)	0.277	0.294	0.072	0.050	0.423	0.099	0.934	0.120
H(N)	0.832	0.378	0.014	0.050	0.285	−0.212	0.571	0.120

TABLE IV

Selected intramolecular distances (Å), angles (°) and torsion angles (°) for (R) NACMBA and (rac) NACMBA (R molecule)

	(R) NACMBA	(rac) NACMBA
C(1)–C(2)	1.501(3)	1.493(7)
C(1)–O	1.218(3)	1.229(4)
C(1)–N	1.331(3)	1.313(5)
C(3)–C(4)	1.528(3)	1.519(7)
C(3)–C(5)	1.511(3)	1.511(6)
C(3)–N	1.459(3)	1.450(6)
C(5)–C(6)	1.374(3)	1.365(6)
C(5)–C(10)	1.375(3)	1.375(7)
C(6)–C(7)	1.382(3)	1.386(8)
C(7)–C(8)	1.347(3)	1.340(9)
C(8)–C(9)	1.368(3)	1.340(1)
C(9)–C(10)	1.370(3)	1.381(9)
N–C(1)–O	123.3(2)	122.1(4)
O–C(1)–C(2)	122.2(3)	120.5(5)
N–C(3)–C(4)	108.7(2)	108.8(4)
C(10)–C(5)–C(6)	118.4(2)	117.2(5)
C(6)–C(5)–C(3)	122.9(2)	123.2(4)
C(7)–C(6)–C(5)	121.0(2)	121.7(6)
C(9)–C(8)–C(7)	120.2(2)	119.8(7)
C(9)–C(10)–C(5)	120.3(2)	120.5(6)
N–C(1)–C(2)	114.5(3)	117.3(4)
N–C(3)–C(5)	113.2(2)	113.1(4)
C(5)–C(3)–C(4)	109.7(2)	110.6(4)
C(10)–C(5)–C(3)	118.7(2)	119.6(5)
C(8)–C(7)–C(6)	119.6(2)	119.9(6)
C(10)–C(9)–C(8)	120.4(2)	121.0(7)
C(3)–N–C(1)	120.9(2)	123.0(4)
H(N)–N–C(1)–O	−176.5(3)	177.7(3)
C(1)–N–C(3)–C(4) = τ_2	−157.8(2)	−154.8(2)
N–C(3)–C(5)–C(6) = τ_1	+31.5(2)	+13.5(3)
C(2)–C(1)–N–C(3)	+176.2(2)	−177.2(2)
C(1)–N–C(3)–C(5)	+80.1(3)	+81.9(2)

2.4 MO Calculations

All geometry optimizations, as well as the interaction energy computations, were achieved using semi-empirical methods (MOPAC 93[16]). PM3 hamiltonian rather than AM1 was chosen because of its better parametrization for nitrogen atom.[17] The results of Molecular Orbitals were analyzed using SYBYL 6.03 (Molecular Modeling Software),[18] interfaced with MOPAC. The initial geometries were extracted from the solids. As recommended,[16] a rotational energy barrier of 60 kJ·mol^{-1} was systematically added for the (CO—NH) linkage ("molecular mechanics correction") in order to represent the planarity of the amide bond.

2.4.1 Molecular Conformation

Because the side chain always appears planar, the conformation of the molecules can be characterized by the torsion angles τ_1 and τ_2, defining respectively the orientation of the phenyl moiety and the rotation around the C3—N bond.

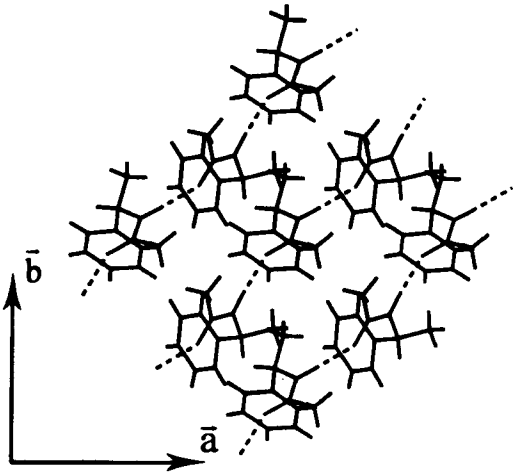

FIGURE 5 Projection along $\bar{c}$ axis of (004) slice in the (R) enantiomer structure of NACMBA showing the CHBMs along ⟨110⟩ direction.

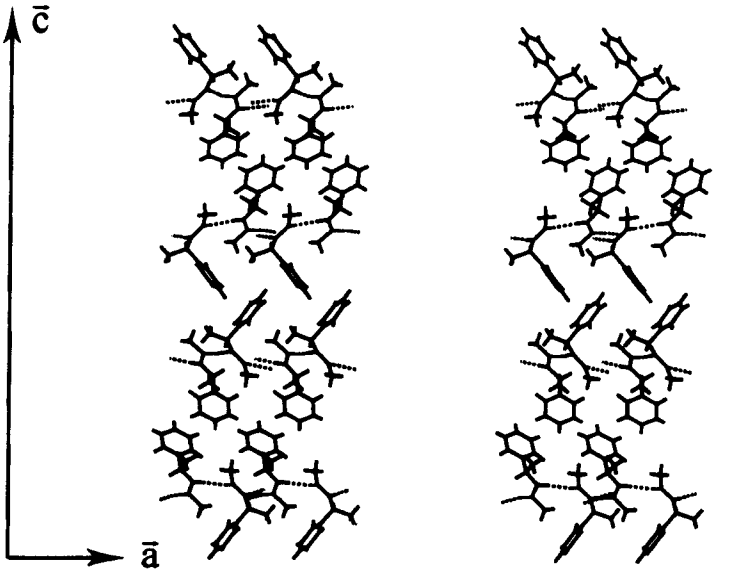

FIGURE 6 Projection along $\bar{b}$ of the (R) enantiomer crystal structure of NACMBA.

Whatever the initial geometry, enantiomer or racemate, it appears that fully optimized geometries in vacuum present only a few differences with the solid states. The lengths of the (C—H) and (N—H) bonds are systematically underestimated in the crystal structures. Table V gathers the observed and calculated values for other

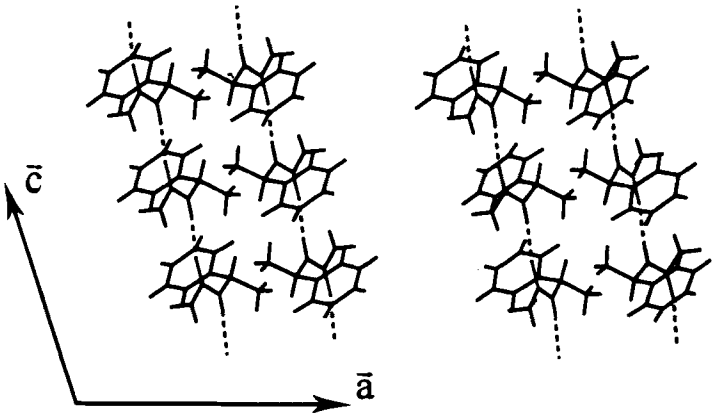

FIGURE 7 Projection along the $\bar{b}$ axis of the racemate crystal structure of NACMBA.

parameters subjected to a major evolution between solid state and fully optimized geometry: τ_1, τ_2 and C1—N bond length. In this table, ΔE is the energy difference between fully optimized conformation and fully optimized conformation except for the considered parameter. The C1—N bond length is significantly longer after the geometry optimization than in solids: (1.331(3)Å for enantiomer, 1.313(5)Å for racemate). This seems to be due to the inability of PM3 parametrization to represent the C—N bond length in *N*-acetyl compounds.

Due to the weak accuracy of the positioning of hydrogen atoms with X-ray diffraction, the relative conformational energies of the molecules in solids have been compared after optimization of all H atom positions (distances, angles and dihedral angles). The molecule, in the pure enantiomer lattice, is found in a more favorable conformation than in the crystal of the racemate ($\Delta E_{conf.} = -17.2\,kJ\cdot mol^{-1}$); nevertheless 45% of this energy is estimated erroneously by PM3 from the stretching energy

TABLE V

Significant conformational differences (and associated energies) between measured (RX) and calculated (PM3) geometries for (R) enantiomer and racemate of NACMBA

	(R) Enantiomer		Racemate	
	RX	PM3	RX	PM3
τ_1(°)	31.5	63.7	13.5*	63.8*
ΔE(kJ·mol^{-1})		−3.9		−7.2
τ_2(°)	−157.8	−139.7	−154.9*	−139.5*
ΔE(kJ·mol^{-1})		−1.0		−0.7
C1–N(Å)	1.33	1.41	1.31	1.41
ΔE(kJ·mol^{-1})		−13.9		−21.6

* Torsion angles calculated for the (R) molecule contained in the racemate.

of the C1—N bond. Thus, a realistic comparison of conformational energy has been carried out by imposing C—N bond lengths at 1.41 Å; this leads to $\Delta E_{conf.} = -9.4\,kJ\cdot mol^{-1}$.

2.4.2 Comparison of R—R and R—S links in solids

Since the main intermolecular links in solids are the hydrogen bonds, we were interested in comparing the relative strength of these H-bonds. For this purpose, we have calculated the hydrogen bond energies E_{Hb} in enantiomer and racemate structures. After optimization restricted to all hydrogen atom positions, the values of E_{Hb} were calculated by the difference between the energy of two H-bonded molecules and the energy of the same but isolated molecules. Table VI contains the values of E_{Hb} and the geometrical characteristics of the H-bonds with (PM3) or without (RX) optimization of the H atoms positions. It can be seen that (R—R) H-bond in enantiomer structure is more stable by $3.7\,kJ\cdot mol^{-1}$ than (R—S) H-bond in racemate. Therefore, the higher thermodynamic stability of the conglomerate at 293 K may be due to a lower conformational energy and also to slightly stronger H-bonds in the enantiomer packing than in racemate packing. The van der Waals contacts, probably of weaker magnitude than the previous terms, cannot reverse the order of stability.

2.4.3 Search for a chiral recognition during the formation of intermolecular H-bonds

Several attempts of full geometry optimization for (R—R) and (R—S) H-bonded associations do not lead to significant energy difference ($< 1\,kJ\cdot mol^{-1}$). The final geometry of these associations shows:

- a hydrogen bond similar to those observed in solids, allowing addition of further H-bonded molecules (i.e. formation of linear CHBMs),
- two additional van der Waals contacts between H atoms:
  - both involving a methyl moiety (of acetyl groups) and a phenyl group in (R—S),
  - one involving a methyl moiety (of acetyl group) and a phenyl group, and the

TABLE VI

Geometric characteristics of hydrogen bonds for R—R (enantiomer) and R—S (racemate) associations in crystal structures (RX) and after geometry optimization restricted to hydrogen atom positions (PM3). Values of E_{Hb} are obtained by a comparison with two isolated molecules whose hydrogen atom positions have been optimized

	Enantiomer (RR)		Racemate (RS)	
	RX	PM3	RX	PM3
d(N···O)(Å)	2.86	2.86	2.87	2.87
d(H···O)(Å)	2.03	1.86	2.10	1.86
(N—H···O)(°)	175.0	170.1	171.8	174.4
E_{Hb}(kJ·mol^{-1})	–	−18.1	–	−14.4

other involving a methyl moiety (of acetyl group) and the C4 methyl group in (R—R).

The angle between the side chain planes is 30° (R—R) and 44° (R—S), which indicates that various geometries can be envisaged for H-bonded associations. As a result, a chiral distinction exists since three distinct intermolecular links are formed; nevertheless, there is no energy difference and hence the relative stability of molecular H-bonded associations in vacuum and also probably in solution cannot be related to the absolute configuration of the molecules.

2.5 Ternary Systems (R)-NACMBA, (S)-NACMBA, Solvent. (Solvent = Toluene or Acetonitrile)

The solubilities have been determined by the following procedure. In a stopped glass thermostated tube (± 0.2 K), the suspension (solute + solvent) is magnetically stirred for 12 h. After sedimentation, the solution is slowly pipetted and then weighed in a stopped flask, previously tarred, with a magnetic stirrer. The solvent of this solution is eliminated by evaporation at 293 K in a well-ventilated area with continuous stirring until constant weight is obtained. Each solid in equilibrium with the saturated solution is identified by routine powder X-ray diffraction and shows the same pattern, identical with pure enantiomer. Table VII lists the solubilities, expressed in mass percent, in toluene and in acetonitrile for various temperatures. In the toluene medium, a significant departure with regard to the ideal behaviour ($\alpha = s_{(\pm)}/s(R) = 2$) arises as soon as the temperature increases from 273 K upwards. Figures 8 and 9 display the solubility curves at 273 K and 287 K in both solvents.

2.6 Preferential Crystallizations

Different attempts were made in toluene and acetonitrile; initial conditions were chosen from solubility curves and supersaturation capacities (Figures 8 and 9). The typical procedures are as follows:

TABLE VII

Solubilities of (R) NACMBA and (±) NACMBA in tolune and acetonitrile

Solvent	T(K)	$s(\pm)$ (% mass)	s(R) (% mass)	α
Toluene	273	2.4	1.0	2.4
	286.3	9.1	1.1	8.3
	287	11.0	1.1	10.0
	288	13.8	1.1	12.5
	301	42.2	2.7	15.8
Acetonitrile	273	20.7	8.6	2.4
	285	37.2	13.3	2.8
	287	41.9	14.9	2.8

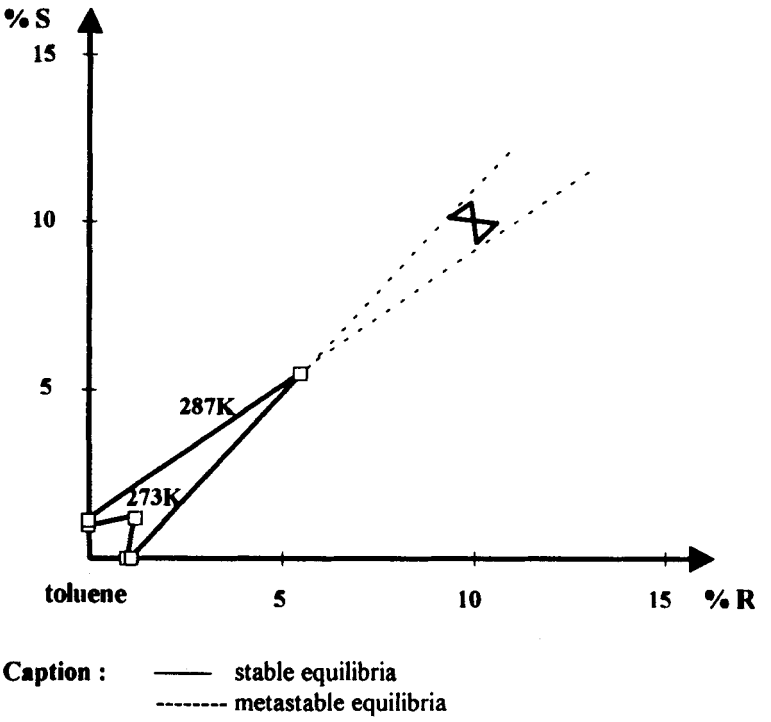

FIGURE 8 Solubility curves at 273 K and 287 K for the ternary system (R) NACMBA-(S) NACMBA-toluene and pathway of preferential crystallization.

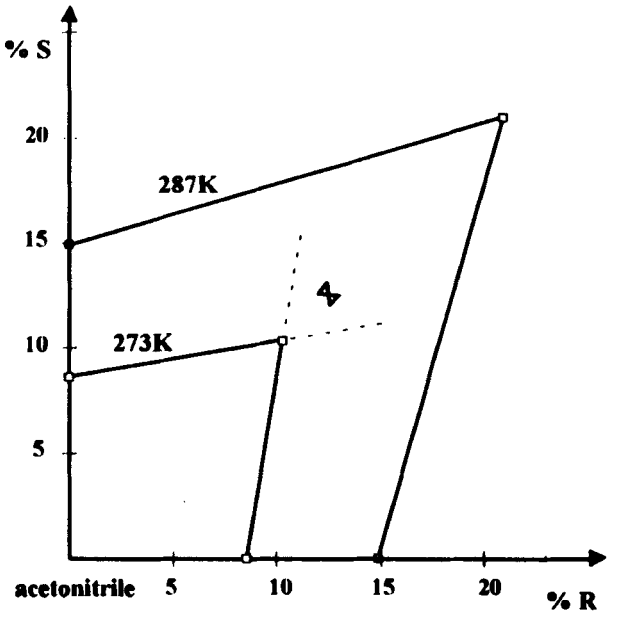

FIGURE 9 Solubility curves at 273 K and 287 K for the ternary system (R) NACMBA-(S) NACMBA-acetonitrile and pathway of preferential crystallization.

2.6.1 *In toluene*

Owing to the shape of the solubility curves, the preferential crystallization has to be performed with a high supersaturation. Fortunately, there is a strong capacity for supersaturation for the racemic mixture in toluene. The overall concentration has been refined so that the spontaneous nucleation of either the conglomerate or the racemate, does not occur within the limit of 1 h.

A mixture made of 5.000 g of (±)NACMBA, 20.0 g of toluene and 0.155 g of (R)NACMBA is heated at 297 K until homogeneity is obtained. The solution, continuously stirred, is cooled down to 287 K and seeded with 4 mg of finely ground and purified (R)NACMBA (O.P. > 99%). Secondary nucleation and growth take place soon after the inoculation and are processed for 12 min. until rapid filtration on porous glass (*n*° 3). The weight (0.35 g) and the optical purity (O.P. = 92%) of the crude crops clearly demonstrate the achievement of the preferential crystallization.

2.6.2 *In acetonitrile*

A mixture made of 3.525 g of (±)NACMBA, 11.5 g of acetonitrile and 0.109 g of (R)NACMBA is thermostated at 279 K until homogeneity is obtained. The solution, continuously stirred, is cooled down to 273 K and seeded with 4 mg of finely ground and purified (R)NACMBA (O.P. > 99%). The crystallization is processed for 40–50 minutes until rapid filtration on porous glass (*n*° 3). The weight (0.20 g) and the optical purity (O.P. = 97%) of the crude crops show that, despite a more favourable α ratio, the yield of the preferential crystallization is not improved.

3. DISCUSSION

3.1 Binary Phase Diagram

To our knowledge, it is the first time that the Tammann graph of a solid-solid invariant in a binary system of enantiomers has been drawn from experiments. This has been made possible because of the proximity of the melting point, and therefore, of a high enough diffusion rate between solid particles. Usually, eutectoids or peritectoids in binary systems of enantiomers, associated with a small enthalpy, are subject to laziness due to a poor diffusion rate and present difficulties in nucleation. However, the experimental values of heat transfers associated with various compositions of this eutectoid could appear fairly scattered with reference to ideal values. This could be justified by the necessity for a complete reconstruction of the CHBMs, from isotactic to syndiotactic, which implies a molecule by molecule process, resembling a mechanism proposed for polymorphic transitions only.[19]

3.2 Ternary Phase Diagrams

The solubility versus the optical purity for various temperatures in toluene and acetonitrile gives some clues about the solute-solvent and solute-solute interactions.

We pointed out that, in toluene, the greater the temperature, the greater the departure from the ideal behaviour. Therefore, the proximity of the melting point of the racemate must be responsible to some extent. Nevertheless, this argument should also hold for acetonitrile which, on the contrary, does not bring about such a discrepancy in the same range of temperature (273 K–287 K). Therefore, the nature of the solvent itself is one of the determinant factors inducing a specific behaviour of the solvated material.

In acetonitrile, the solubility is higher than in toluene, whatever the temperature. This has to be related to the dual ability of acetonitrile to solvate polar and apolar species; the solvation might therefore be achieved by means of interactions involving all parts of the solute. The interactions NACMBA-acetonitrile must be strong enough and independent of the absolute configuration of the solute, so that the enantiomers are solvated as monomers and only a slight departure from ideal behaviour is detected.

In a non-polar solvent such as toluene, the lower solubility can be attributed to the difficulty of solvation of the polar part of the solute molecules. A consequence of this difficulty could be the promotion of Chains of Hydrogen-Bonded Molecules (CHBMs) by the following dynamic equilibrium:

$$k(\mathrm{R})_{\text{solvated}} + l(\mathrm{S})_{\text{solvated}} \Leftrightarrow \mathrm{CHBM}(k\mathrm{R} + l\mathrm{S})_{\text{solvated}}.$$

Hence, it is likely that these CHBMs existing in solution have a structure resembling those observed in the crystal structures of the enantiomer and racemate, but, as we will see below, progressively less tactic as the optical purity of the solution evolves from 100% to 0%.

The dimension of these linear aggregates (i.e. the value of $n = k + l$) depends upon two different parameters:

1. The temperature: the higher the temperature the smaller the n value this results from a better solvation at high temperature and because of the entropic factor.
2. The solvent: we have previously postulated that the existence of CHBMs was associated with non-polar solvents, whereas such molecular associations were not justified in a solvent like acetonitrile. In fact, we may assume that there exists a continuous variation of n versus the polarity of the solvent: the smaller the polarity, the higher the value of n.

The tacticity of the CHBMs depends upon the optical purity of the solution: assuming the existence of the CHBMs in a non-polar solvent, these chains are isotactic for pure enantiomers solutions only (OP = 100%). As soon as the counter enantiomer is added to the solution, the dynamic equilibrium postulated above brings about the presence of the counter enantiomer in the CHBMs. This result is consistent with our calculation; we found no energy difference in vacuum (and in an apolar solvent) between H-bonded associations R—R and R—S. This means that the non-polar solvent promotes the formation of these CHBMs regardless of the chirality of the constitutive molecules. Therefore, for a racemic solution (OP = 0%), these chains should exhibit an atactic character.

3.3 Interactions Between CHBMs and Departure from the Ideal Behaviour

As no decisive recognition is made during the formation of CHBMs in toluene, the large departure from the ideal behaviour probably results from the interactions between the CHBMs. If the optical purity of the solution equals 100%, the CHBMs could match very well with stable and periodic interactions as in enantiomer structure; this results in low solubility. On the contrary, for atactic chains, the fit is less efficient because the random distribution of Rand S molecules induces sterical hindrances, and hence, weaker interactions between neighbouring CHBMs.

Nevertheless, at low temperature, CHBMs have sufficient energy of interaction, whatever their tacticity, to assemble (thus $\alpha \approx 2$).

As temperature increases, the atactic CHBMs break apart in the solution (i.e. sharp increase of solubility of racemic mixture) whereas isotactic CHBMs, more strongly secured together, are less affected (i.e. little increase in solubility of the enantiomer in the same range of temperature, cf. Table VII) because of their stronger interactions. Hence, $\alpha \gg 2$ as soon as the threshold of 273 K, defining the coalescing limit of atactic CHBMs, is exceeded.

3.4 Nucleation of the Racemate and Preferential Crystallization

Reproducible experiments have shown that the racemate can be obtained by rapid cooling to 273 K of a previously homogenized racemic solution at 25% in toluene. This is due to the relative stability of this phase with regard to the conglomerate in this domain of temperature (metastable equilibrium). In addition, we have the following statement: at high supersaturation (σ) of racemic solution, the nucleation rate of the racemate prevails over the nucleation rate of the conglomerate because of the absence of segregation during crystallization of the racemate and because no solid solution has been detected. Indeed, the diffusion (and the resulting incorporating rate) of R and S enantiomers towards their nuclei made of molecules of the same chirality is slower than the diffusion of R and S molecules towards nuclei which can incorporate both chiralities.

In mild conditions of nucleation and crystal growth (low σ), the racemate does not interfere with the secondary nucleation and crystal growth of the enantiomer, as exemplified by the two achievements of preferential crystallization. Because of the limitation of the metastable solubility curves in toluene (Figure 8), the domain in which the resolution can be performed is very narrow. In acetonitrile, despite a wider domain, the yield (Figure 9) is almost the same as in toluene.

Although the interactions between solute and solvent and between opposite enantiomers are different in toluene and in acetonitrile, the small difference in the efficiency of the resolution process seems to indicate that the difficulty encountered in implementation is in connection with the mechanism of growth itself. As soon as the solution contains an excess of a given enantiomer, the growth of the counter enantiomer is slowed down to such an extent that the entrainment effect is rapidly stopped. In that situation, a crystal of the R enantiomer could exhibit sufficiently strong "racemate-like" R—S interactions at its interface as soon as the solution contains an excess of S. The higher the S enantiomeric excess, the greater the slowing down of crystal growth of the R enantiomer and the greater the probability of secondary nucleation of the S enantiomer.

4. CONCLUSION

Different kinds of interactions between (R) and (S) *N*-Acetyl-α-Methylbenzylamine have been pointed out in solid state and in solution. Up to 337 K, the conglomerate is stable and the racemate is metastable; above 337 K, the situation is reversed. The transition through an eutectoid invariant is determined by calorimetry and high temperature X-ray diffraction.

Both structures have been solved by X-ray diffraction on single crystals. Chains of H-bonded molecules are found in both cases, isotactic in enantiomer, syndiotactic in racemate. These chains are held together by van der Waals contacts. The two packings have almost the same compacity at 293 K.

Using conformations existing in solids, M.O. calculations (PM3 hamiltonian) have shown that the higher stability of the conglomerate at 293 K is mainly due to a conformational contribution, and, to a lesser extent, to intermolecular (H-bond) forces. Comparative computations suggest that, from an energetic point of view, no chiral selectivity exists in vacuum between (R—R) and (R—S) H-bonded molecular associations.

In solution, the departure from the ideal behaviour depends on three factors: temperature, optical purity and solvent. Apolar solvents promote the formation of CHBMs by means of a dynamic equilibrium between solvated molecules of solute. These putative chains are isotactic if OP = 100% and atactic if OP = 0%. The departure is due to different interactions between CHBMs versus optical purity, inducing different behaviours with increasing temperature.

For quasi-racemic solutions out of equilibrium processes lead to different results according to the degree of supersaturation (σ):

- If σ is very high, racemate can spontaneously nucleate,
- If σ is below the limit of spontaneous nucleation of the racemate, preferential crystallization can be achieved. The poor yield does not seem to be affected by the nature of the solvent. Considering the relative stability of the racemate versus the conglomerate, the R—S interactions are just slightly less stable than the R—R interactions at solid interface; the former could play a key role as soon as the enantiomeric excess of the solution deviates from 0.

Acknowledgements

Thanks are due to F. Robert (Laboratoire de Chimie des métaux de transition, Université de Paris VI) for help in the resolution of the racemate crystal structure.

References

1. B. S. Green and M. Knossow, *Science*, **214**, 795 (1981).
2. R. J. Davey, S. N. Black, L. J. Williams, D. McEwan and D. E. Sadler, *J. Crystal. Growth*, **102**, 97 (1990).
3. G. Coquerel, G. Perez and P. Hartman, *J. Crystal. Growth*, **88**, 511 (1988).
4. P. Newman, *Optical Resolution Procedures for Chemical Compounds, Amines and Related Compounds* (Manhatan College, New York, 1978), **1**, 79–84.
5. M. Nokamura, T. Shiraiwa and H. Kurokawa, *Technol. Rep. Kansai Univ.* **27**, 111 (1986).
6. H. Nohira, M. Kai, M. Nohira, J. Nishikawa, T. Hoshiko and K. Saigo, *Chem. Lett.*, **7**, 951 (1981).

7. A. Collet, M. J. Brienne and J. Jacques, *Bull. Soc. Chim. Fr.*, **1**, 127 (1972).
8. R. L. Scott, *J. Chem. Soc. Faraday Trans. II*, **3**, 356 (1977).
9. A. Boultif and D. Louër, *J. Appl. Cryst.*, **24**, 987 (1991).
10. I. Prigogine and R. Defay, *Thermodynamique Chimique* Desoer, Liège, (1950).
11. I. Schröeder, *Z. Phys. Chem.*, **11**, 449 (1893).
12. J. J. Van Laar, *Arch. Neerl.*, **II**, 8, 264 (1903).
13. G. M. Sheldrick, *SHELXS-86, Program for structure solution*, Gottingen, (1986).
14. P. Hartman, *Modern PBC theory, in: Morphology of Crystals*, Part I ed. I. Sunagawa, Terra, Tokyo, 269–319 (1987).
15. C. P. Brock, W. B. Schweizer and J. D. Dunitz, *J. Am. Chem. Soc.*, **113**, 9811 (1991).
16. J. J. P. Stewart, *MOPAC 93.00 Manual* Fujitsu Limited, Tokyo, Japan, (1993).
17. I. Juranic, H. S. Rzepa and M. Y. Yi, *J. Chem. Soc. Perkin Trans. II*, 877 (1990) and references therein.
18. SYBYL, Molecular Modeling Software (Version 6.03, 1993), Tripos Associates, St. Louis, MO.
19. Y. M. Mnyukh, *Mol. Cryst. Liq. Cryst.*, **52**, 163 (1979).